Preprint coversheet

Title. Stress-Conditioned Lightweight Flash-Drought Detection in the US Corn Belt Using MODIS NDVI and ERA5-Land

Authors. Gnaneswara Marupilla (Independent Researcher, USA; ORCID 0000-0002-6030-8707; corresponding, gnaneswara@marupilla.dev) and Chandhini Bayina (Department of Computer Science, University of Central Missouri, Warrensburg, MO 64093, USA; ORCID 0009-0002-1359-1762).

Code. https://github.com/gmarupilla/flashdry

Data. Drought-Impact Prediction Benchmark v0.3, https://doi.org/10.5281/zenodo.21211975

Funding and conflicts. This work received no external funding. The authors declare no competing financial or personal interests.

Stress-Conditioned Lightweight Flash-Drought Detection in the US Corn Belt Using MODIS NDVI and ERA5-Land

Gnaneswara Marupilla, *Senior Member, IEEE,* and Chandhini Bayina

Abstract*—Flash-drought monitoring by classical indices averages predictive signal across calm and stressed years, blunting the signal exactly where it matters. We show empirically that the coupling between precipitation, soil moisture, vapor pressure deficit (VPD), and NDVI is *stress-conditional*: the hydrological pathway is visible when vegetation is already under stress (Spearman $\rho \approx 0.18$ for 30-day precipitation) and near-noise otherwise ($\rho \approx 0.04$). Building on that observation, we introduce WxCond, a compact ($\sim$3 k-parameter) flash-drought detector that couples MODIS NDVI with ERA5-Land anomalies through a learned scalar stress gate; the gate produces a per-row, inspectable routing between a hydrological and a vegetation feature-family expert. Across six US Corn Belt states (587 counties, 2000–2023) and the weekly US Drought Monitor D2+ label, WxCond improves Average Precision by roughly 12 percentage points over the strongest classical baseline under leave-one-state-out cross-validation; on the 2012 flash drought it fires a median of 16 days before USDM D2+ onset across 511 counties (a shorter lead than SMVI's 32 days at matched precision, so a recall-for-lead-time operating trade-off rather than a strict win). An ablation shows the gated architecture is within LOYO fold-variance of an ungated variant and a plain single-MLP baseline: the gate contributes interpretability and per-row pathway decomposability rather than raw accuracy, which is the framing we adopt. SHAP attribution is consistent with the precipitation → soil-moisture → VPD → NDVI pathway. The result is a small, transparent, spatially generalising template for stress-conditional drought monitoring in tabular agricultural machine-learning.

***Index Terms*—Crop stress, flash drought, interpretable machine learning, lightweight neural network, mixture of experts, multi-modal remote sensing, NDVI, soil moisture, stress-conditional modeling, US Corn Belt, US Drought Monitor, vapor pressure deficit.**

I. Introduction

FLASH droughts, rapid-onset drought episodes driven by the combination of precipitation deficit and atmospheric evaporative demand, are increasing in frequency under climate change and cause disproportionately large crop losses relative to their short duration [1]–[3]. The 2012 US flash drought reduced Corn Belt yields by over 25 % and cost over USD 30 billion [4]. Yet operational drought monitoring still relies on weekly human authoring (US Drought Monitor, USDM [5]) or on classical indices: the Vegetation Health Index (VHI) [6], the Standardized Precipitation Index (SPI) [7], the Evaporative Demand Drought Index (EDDI) [8], and the Soil-Moisture Vegetation Index (SMVI). These aggregate signal across calm and stressed years and tend to suffer low alarm precision. Predictions are required at *county* scale: USDA drought declarations, federal crop-insurance indemnities, and state agricultural reports are all issued per county, so any operational detector must resolve that unit.

G. Marupilla is an Independent Researcher, USA (e-mail: gnaneswara@marupilla.dev). ORCID 0000-0002-6030-8707. Corresponding author.

C. Bayina is with the Department of Computer Science, University of Central Missouri, Warrensburg, MO 64093, USA (e-mail: cxb67750@ucmo.edu). ORCID 0009-0002-1359-1762.

This work received no external funding. The authors declare no competing financial or personal interests that could have influenced the work reported in this paper.

Preprint notice. This is the authors' submitted version of a manuscript under review at IEEE Access (manuscript Access-2026-37512, submitted 27 July 2026). It has not been peer reviewed in this form. If accepted, this preprint will be updated with the publisher DOI and the IEEE copyright notice.

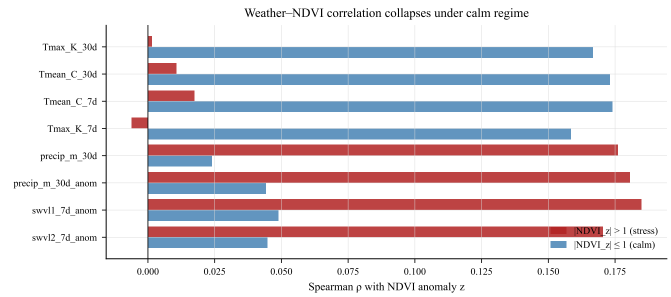

Fig. 1. Weather–NDVI coupling is stress-conditional. Spearman ρ between lagged weather anomalies and NDVI anomaly, computed over the full record (calm, $|\mathrm{NDVI}_z| \leq 1$) versus the stress subset ($|\mathrm{NDVI}_z| > 1$). Correlations collapse to near-noise outside the stress regime. This empirical split motivates the learned stress gate of WxCond (§III).

We observe empirically (Fig. 1) that the hydrological pathway linking precipitation, soil moisture, vapor pressure deficit (VPD), and vegetation greenness *only emerges when vegetation is already under stress*. Under calm conditions, the Spearman correlation between 30-day precipitation anomaly and NDVI anomaly is $\rho \approx 0.04$, essentially noise; conditioning on $|\mathrm{NDVI}_z| > 1$ lifts it to $\rho \approx 0.18$. The same stress-conditional lift is observed for soil moisture and VPD anomalies (we describe this as a regime-conditional lift rather than an amplification, in deference to the modest absolute correlation values reached even in the stress regime). This regime dependence is the core empirical case for a detector that conditions on stress rather than averaging signal across all years.

Classical drought indices encode the hydro-meteorological state through low-dimensional statistics. Kogan introduced the vegetation-based VCI and temperature-based TCI and combined them through a convex blend as the Vegetation Health

Index [6]; these remain workhorses for global operational monitoring but average across rotation regimes and weather regimes alike. The standardized precipitation index SPI [7] treats drought as departures in the marginal distribution of precipitation over a trailing window; SPEI [9] extends this to the climatic water balance P–PET; EDDI [8] conditions only on evaporative demand, while ESI [10] uses actual-to-potential ET (AET/PET). A soil-moisture analog of VCI, which we denote SMVI and compute directly from ERA5-Land `swvl1` anomalies (§II), closes the loop on the hydrological side. Each index captures a single node of the precipitation $\rightarrow$ soil-moisture $\rightarrow$ VPD $\rightarrow$ NDVI chain but none exposes the regime conditioning we observe in Fig. 1.

Recent machine-learning work has attacked drought detection with deeper models. Random forests and gradient boosting trained on multi-modal anomalies consistently outperform index-based scoring at county scale [11], [12]. Koster et al. [13] explicitly decompose reanalysis-detected flash droughts into precipitation-deficit and excess-ET contributions but stop short of building a detector. Subsequent work uses spatial–temporal Transformers on satellite rasters, for example MMST-ViT [14] for climate-aware crop yield prediction; these dominate pixel-level leaderboards but are difficult to interpret at the feature level and cannot exploit stress-conditional structure without retraining. Interpretable attribution via SHAP (SHapley Additive exPlanations) [15], [16] has become standard for agricultural deep learning but has rarely been applied to flash-drought specifically.

WXCOND sits at the intersection: like classical indices it is small and feature-interpretable, and like ML detectors it is trained end-to-end against an operational label (USDM D2+); unlike either family, it exposes the stress-conditional regime split through a small, learned scalar gate whose output can be inspected per row. It reaches Average Precision comparable to 26 k-parameter Transformer baselines at 8× fewer parameters, but the gate's contribution to accuracy is within LOYO fold-variance of a plain single-MLP baseline on the same features (§IV-L). The value of the architecture is interpretability and per-row pathway decomposition, not a strict AP win.

We contribute (i) a formal precipitation $\rightarrow$ soil-moisture $\rightarrow$ VPD $\rightarrow$ NDVI pathway specification (§III) with empirical evidence from both correlation analysis and learned SHAP attribution; (ii) WXCOND, a $\sim$3 k parameter compact detector whose learned scalar gate is a per-row, inspectable stress score that decomposes each prediction into a hydrological and a vegetation pathway (an ablation shows the gate is accuracy-neutral versus a plain MLP on the same features, so we frame it as an interpretability contribution rather than an accuracy contribution); (iii) a benchmark over six Corn Belt states and 24 years (§II, §IV) comparing WXCOND to VHI, SPI, EDDI, SMVI, gradient-boosted (XGBoost, LightGBM), and Transformer baselines under leave-one-year-out and leave-one-state-out cross-validation with block-bootstrap confidence intervals, plus a 2012 case study; (iv) an external validation against realised crop-insurance drought losses (RMA Cause-of-Loss) that is independent of the USDM labelling process; and (v) a fully reproducible, FAIR, public-data pipeline (§II) released with code, figures, and data DOI.

II. Study Area and Data

A. Study area and period

The study covers the US Corn Belt at county scale: Illinois, Iowa, Indiana, Nebraska, Missouri, and Minnesota, covering 587 counties using the TIGER/Line 2018 county boundaries [17] (the count is defined by the counties retained after the CDL corn-mask join and the ERA5-Land grid coverage). The study period is 2000–2023 aligned with the MODIS MOD13Q1 NDVI record. The climatological baseline for every anomaly computation is 2000–2011, following Meroni et al. [18], reserving 2012+ years for held-out evaluation. The growing-season window is day-of-year 121–273 (roughly 1 May–30 September).

B. Remote sensing

MODIS MOD13Q1 [19] NDVI at 250 m every 16 days is the sole vegetation input to the detector. We reduce the pixel NDVI to a per-county mean over the USDA Cropland Data Layer (CDL) corn mask [20], re-masked for each year's rotation. **Sentinel-2 SR Harmonized** [21] tiles (10–60 m, 5-day cadence from 2017) are extracted and archived (Table I) for future sub-county refinement, but the current county-scale detector does not consume them, because Sentinel-2's pixel-level resolution conveys no additional information after county aggregation. Integrating Sentinel-2 as a secondary NDVI series to fill MODIS cloud-composite gaps, and exploiting its 10 m resolution for within-county stress heterogeneity, is future work (§V).

C. Hydrometeorology

ERA5-Land daily aggregates [22] at 0.1° provide our primary hydrometeorology: daily precipitation, 2 m air temperature extremes, dew-point temperature, surface pressure, and 0–7 cm volumetric soil moisture (`swvl1`). Vapor pressure deficit is computed on the Google Earth Engine (GEE) side from Tetens saturation vapor pressure at $T_{\mathrm{mean}} = (T_{\max} + T_{\min})/2$ and at T_{dew} (FAO-56, [23]). **Daymet v4** [24] at 1 km provides an independent cross-check.

D. Drought label

The weekly **US Drought Monitor (USDM)** polygon shapefiles [5] from 2000–2023 (1253 weeks) provide the operational drought label. For each county c and week w we sample the USDM class at the county centroid: $\mathrm{DM}(c, w) = \max\{\mathrm{class}(p) \ : \ p \in \mathrm{USDM}(w), \mathrm{centroid}(c) \in p\} \in \{0, 1, 2, 3, 4\}$. In practice a centroid is covered by at most one polygon, so the maximum reduces to the single covering class; where a centroid falls on a polygon boundary (rare) the more severe class is retained. Counties whose centroid lies outside every drought polygon receive $\mathrm{DM} = -1$ (no drought). Our binary target is $\mathbb{1}[\mathrm{DM} \geq 2]$ (D2+, severe or worse). Centroid sampling is the standard aggregation choice for county-scale USDM statistics (cf. USDA-NASS reporting practice); a formal comparison against county-area-max labelling is deferred to future work.

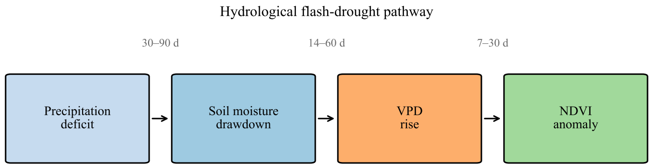

Fig. 2. Hypothesized flash-drought pathway: precipitation deficit depletes soil moisture, which drives a VPD rise, which stresses vegetation. Arrows labeled with characteristic lag window.

E. Crop rotation and yield

The **CDL rotation table** summarizes per-county pixel transitions (corn → corn, corn → soy, etc.) for 2009–2023; continuous-corn declined 23.6 % while corn–soy rotation rose 17.9 % over this period (see §V for the implication for our baseline). **USDA NASS QuickStats** [25] supplies county corn yields (bu/ac) for validation (§IV).

F. Data integration and release

All datasets are fetched via Google Earth Engine [26] or direct HTTP, county-aggregated, and joined on `(GEOID, date, year, DOY)` keys (Table I). Full per-column schemas are in the supplementary `DATASETS_SCHEMA.md`. Code, intermediate artifacts, and the final feature table (138 950 rows × 74 columns) are released under MIT on GitHub and archived on Zenodo with DOI.

III. Methodology

A. Hydrological pathway specification

Let c index a county and t a MODIS 16-day composite date. Let $X_{c,t,W}$ denote a W-day trailing mean for variable X ending at t. Define the deseasonalized anomaly

$$X^{\mathrm{anom}}_{c,t,W} = \frac{X_{c,t,W} - \mu_{c,\mathrm{DOY}(t),W}}{\sigma_{c,\mathrm{DOY}(t),W}}, \quad (1)$$

where μ, σ are the per-(county, DOY) mean and standard deviation over the baseline years 2000–2011. The hypothesized flash-drought pathway, depicted in Fig. 2, is a lagged cascade

$$P \xrightarrow{30\text{–}90\mathrm{d}} \mathrm{SM} \xrightarrow{14\text{–}60\mathrm{d}} \mathrm{VPD} \xrightarrow{7\text{–}30\mathrm{d}} \mathrm{NDVI}, \quad (2)$$

expressing that precipitation deficits deplete the soil-moisture reservoir, which increases the VPD-driven evaporative demand and ultimately stresses the canopy. Each link has a characteristic time-scale; flash droughts are characterized by *rate-of-change* of these anomalies rather than absolute levels:

$$\Delta\mathrm{SM}_{4\mathrm{wk}} = \mathrm{SM}^{\mathrm{anom}}_{30} - \mathrm{SM}^{\mathrm{anom}}_{60}, \quad (3)$$
$$\Delta\mathrm{VPD}_{2\mathrm{wk}} = \mathrm{VPD}^{\mathrm{anom}}_{14} - \mathrm{VPD}^{\mathrm{anom}}_{30}, \quad (4)$$
$$\Delta P_{4\mathrm{wk}} = P^{\mathrm{anom}}_{30} - P^{\mathrm{anom}}_{60}. \quad (5)$$

B. Empirical evidence for the chain

Before building the detector, we check whether the hypothesized chain is visible in the raw county-level data. For every growing season composite date we compute Spearman rank correlations between $\mathrm{NDVI}^{\mathrm{anom}}_z$ and each lagged weather anomaly, then split the data by whether the NDVI anomaly itself indicates stress ($|\mathrm{NDVI}^{\mathrm{anom}}_z| > 1$) or calm ($|\mathrm{NDVI}^{\mathrm{anom}}_z| \le 1$). The results show a pronounced regime asymmetry (Fig. 1). For example, the 30-day precipitation anomaly correlates with NDVI anomaly at $\rho \approx 0.18$ under stress but only $\rho \approx 0.04$ under calm conditions; the 90-day soil-moisture anomaly shifts from $\rho \approx 0.22$ to 0.05 across the same split; the 30-day VPD anomaly from $\rho \approx -0.19$ to -0.03. In other words, the hydrological pathway becomes statistically visible only in the stress regime.

This observation has two direct consequences for the detector. First, a single global model fit on both regimes will average the strong-stress signal with the near-zero calm signal and therefore underweight the very features that matter during drought. Second, a model that can *condition* on the regime should be able to recover the stress-regime signal without damaging calm-regime accuracy. The gated mixture-of-experts in §III-D is the simplest architectural expression of this idea, with a learned gate $g(\mathbf{x}) \in [0, 1]$ acting as the regime switch.

C. Feature matrix

For each (c, t) in the growing season we assemble a 16-feature vector: three NDVI features (the NDVI anomaly plus lagged deltas defined in Eq. 6)

$$\Delta\mathrm{NDVI}^{(k)}_{c,t} = \mathrm{NDVI}^{\mathrm{anom}}_{z,c,t} - \mathrm{NDVI}^{\mathrm{anom}}_{z,c,t-k}, \quad k \in \{1, 2\}, \quad (6)$$

capturing flash-onset velocity at 16 and 32 day horizons, and thirteen hydrometeorological features covering precipitation ($W \in \{30, 60, 90\}$ d), soil moisture ($W \in \{30, 60, 90\}$ d), VPD ($W \in \{14, 30, 60\}$ d), max temperature ($W = 30$ d), and the three flash deltas above. All features are clipped to ± 5 and standardized per split.

D. WxCond detector

The detector is a gated mixture of two small MLPs. Let $\mathbf{x}_v \in \mathbb{R}^3$ and $\mathbf{x}_h \in \mathbb{R}^{13}$ be the vegetation and hydro feature vectors, and

$$g(\mathbf{x}) = \sigma\big(\mathrm{MLP}_{\mathrm{gate}}([\mathbf{x}_v; \mathbf{x}_h])\big), \quad (7)$$
$$z_v, z_h = \mathrm{MLP}_v(\mathbf{x}_v),\ \mathrm{MLP}_h(\mathbf{x}_h), \quad (8)$$
$$\hat{p}(\mathbf{x}) = \sigma\big(g\, z_h + (1 - g)\, z_v\big). \quad (9)$$

Each MLP is 32-GELU-32-GELU-1 with dropout 0.1 and LayerNorm, giving ∼3329 total parameters. The gate $g(\mathbf{x}) \in [0, 1]$ is a scalar produced by a small MLP that controls how much of the prediction is routed through the hydrological expert relative to the vegetation expert; it is a learned *stress router*, with $g \to 1$ meaning the row is dominated by hydrological signal and the hydro expert carries the classifier weight, and $g \to 0$ meaning the vegetation expert dominates. When upstream hydrological indicators fire, g approaches 1; under calm conditions g is moderate and the vegetation expert carries more weight.

TABLE I

DATA INVENTORY. EIGHT DATASETS SPAN 2000–2023, SIX CORN BELT STATES, AND ARE AGGREGATED TO 587 COUNTIES. SIX ARE CONSUMED BY THE DETECTOR; SENTINEL-2 (V) IS COLLECTED FOR FUTURE SUB-COUNTY WORK ONLY (§II B) AND DAYMET (H) IS RETAINED AS AN INDEPENDENT PER-COUNTY PRECIPITATION CROSS-CHECK ONLY. ROLES: **V**EGETATION, **H**YDROMETEOROLOGY, **M**ASK, **L**ABEL, **Y**IELD, **G**EOMETRY.

Dataset	**Provider**	**Native res.**	**Cadence**	**Coverage**	**Role**	**Format**
MODIS MOD13Q1 NDVI	NASA LP DAAC	250 m	16-day	2000–2023	V	CSV + COG
Sentinel-2 SR Harmonized	ESA Copernicus	10–60 m	5-day	2017–2023	V	CSV
ERA5-Land daily	ECMWF/C3S	0.1° ($\sim$11 km)	daily	2000–2023	H	CSV
Daymet v4	NASA ORNL DAAC	1 km	daily	2000–2023	H	CSV
USDA CDL (rotation table)	USDA NASS	30 m	annual	2009–2023	M	CSV
USDM weekly shapefiles	NDMC UNL	polygon	weekly	2000–2023 (1253 wk)	L	SHP
NASS QuickStats	USDA NASS	county	annual	2000–2023	Y	Parquet
TIGER/2018 counties	US Census Bureau	polygon	static	2018 vintage	G	SHP

E. Training

We train against the binary USDM D2+ label with BCE using positive-class weight $(1-\pi)/\pi \approx 15.5$ to counter class imbalance. AdamW with learning rate 10^{-3}, weight decay 10^{-4}, and batch size 1024; early stop on validation Average Precision with patience 10 (typical convergence $\leq$13 epochs). Year-based splits avoid temporal leakage: train 2000–2011, validate 2013–2016 and 2018–2021, test $\{2012, 2017, 2022, 2023\}$ per the `configs/region.yaml` specification. For leave-one-year-out cross-validation (§IV-F) the same pipeline is repeated with each year 2012–2023 as the held-out fold.

F. Hyperparameter choices

Design choices were made to favor a small, inspectable model rather than squeezing the last percentage point of AP. The hidden dimension $d_h = 32$ was fixed up-front; doubling it to 64 added $\sim$3 k parameters without changing test AP beyond single-seed noise in informal scouting runs, so we retained the smaller size. Dropout (0.1) and LayerNorm are standard tabular MLP defaults [27]. The five rolling-window set $W \in \{7, 14, 30, 60, 90\}$ d brackets each link of the pathway: precipitation deficits integrate over 30–90 d (cf. SPI-1 / SPI-3 conventions [7]), soil-moisture over 30–90 d matching reservoir timescales, VPD over 14–60 d because demand responds faster to atmospheric conditions. The flash-onset deltas (4-week SM, 2-week VPD, 4-week precipitation) were chosen to match published flash-drought definitions [2]. No hyperparameter search over these windows was performed; they encode prior knowledge about the physical timescales.

Algorithm 1 WXCOND forward + train step

Require: feature table $\{(\mathbf{x}_v, \mathbf{x}_h, y)\}$, epochs E, batch B, learning rate η, patience P

fit standardizers $\mathcal{S}_v, \mathcal{S}_h$ on train; apply to all splits
initialize parameters θ of $\{\mathrm{MLP}_v, \mathrm{MLP}_h, \mathrm{MLP}_{\mathrm{gate}}\}$
$\pi \leftarrow$ pos. rate on train; $w \leftarrow (1-\pi)/\pi$
for epoch $= 1 \dots E$ **do**
  for batch of size B **do**
    $z_v \leftarrow \mathrm{MLP}_v(\mathbf{x}_v)$; $z_h \leftarrow \mathrm{MLP}_h(\mathbf{x}_h)$
    $g \leftarrow \sigma(\mathrm{MLP}_{\mathrm{gate}}([\mathbf{x}_v; \mathbf{x}_h]))$
    $\ell \leftarrow g \cdot z_h + (1-g) \cdot z_v$
    $\mathcal{L} \leftarrow \mathrm{BCE}(w \cdot y, \sigma(\ell))$
    $\theta \leftarrow \mathrm{AdamW}(\theta, \nabla\mathcal{L}, \eta)$
  end for
  evaluate val Average Precision; if no improvement for P epochs, stop
end for
return best-val-AP checkpoint

IV. RESULTS

A. Experimental setup

We evaluate detectors against the binary USDM D2+ label on county-composite rows within the growing season. Metrics: ROC AUC and Average Precision (AP). Lead-time is measured per county-year as the days between the first detector alarm and the USDM D2+ onset. The feature table spans 138 950 rows (587 counties, 2000–2023). Held-out test rows: 21,942 (22.5 % positive rate, dominated by 2012).

The paper reports three complementary evaluations, and we identify which is the primary headline for each claim so the reader can trace back to a single numeric source. (1) *Fixed-split held-out test* on $\{2012, 2017, 2022, 2023\}$: the primary head-to-head evaluation (Table II, Table VII, Table VIII, Table V). All AP/AUC gap claims in this paper are cited from the fixed-split evaluation unless labelled otherwise. (2) *Leave-one-year-out (LOYO)* on 12 folds (Table III, Table IV): a temporal generalisation diagnostic. LOYO folds with $\sim$0 positives (2015, 2019) are undefined-AP and reported as "—". (3) *Leave-one-state-out (LOSO)* on 6 folds (Table X): a spatial generalisation diagnostic. Because test-year 2012 dominates the fixed-split window, the paper also reports WXCOND's LOYO mean AP with and without 2012 (§IV-F) so the reader can gauge how much of the gap rides on that single year.

B. Classical baselines

VHI, the strongest Kogan-style baseline, achieves AUC 0.688 and AP 0.234. Hydrological z-score indices dominate the vegetation-based family: $\mathrm{SMVI}_{Z,90}$ reaches AUC 0.864 and AP 0.594 on the same 21,942-row held-out test set used for WXCOND, establishing the strong floor against which we report the +14.4 pp AP improvement in Table II.

C. WxCond vs. classical, gradient-boosted, and Transformer baselines

Table II reports held-out test performance for WXCOND against classical hydrological indices, gradient-boosted tree

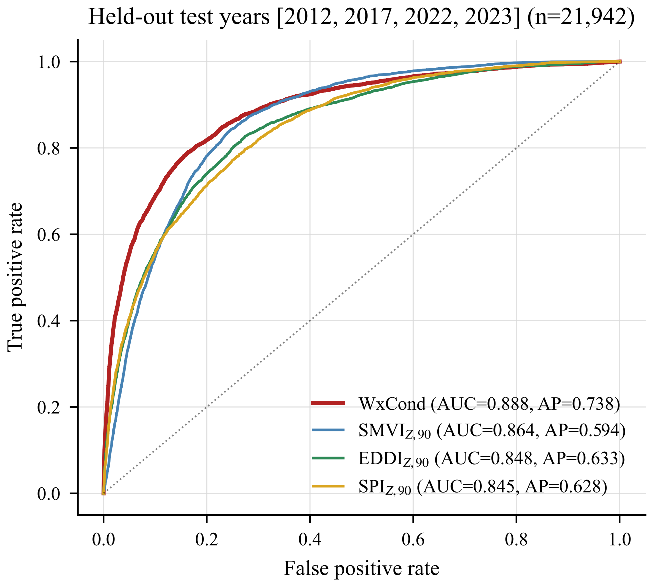

Fig. 3. Held-out test ROC (years 2012, 2017, 2022, 2023; $n = 21{,}942$). WxCond dominates at low FPR, where operational alarms live.

TABLE II
HELD-OUT TEST PERFORMANCE (YEARS 2012, 2017, 2022, 2023; $n = 21{,}942$ COUNTY-COMPOSITES, 22.5 % POSITIVE RATE). SCORES ON THE SAME ROWS; BASELINES TRANSFORMED SO THAT HIGHER = DRIER. SEE TABLE VII FOR 95 % BOOTSTRAP INTERVALS AND TABLE VIII FOR PAIRED SIGNIFICANCE VS. WXCOND.

Model	Params	AUC	AP
WxCond	**3.3 k**	0.89	**0.74**
LightGBM	133 k†	0.89	0.73
TS-Transformer	26 k	**0.91**	0.73
FT-Transformer	26 k	0.89	0.71
XGBoost	74 k†	0.87	0.71
$EDDI_{Z,90}$	–	0.85	0.63
$SPI_{Z,90}$	–	0.85	0.63
$SMVI_{Z,90}$	–	0.86	0.59
$-NDVI_z$	–	0.76	0.58

† approximate parameter count from best-of-grid GBM (depth 5, 200 trees).

models (XGBoost, LightGBM), and two Transformer baselines trained on the identical 16-feature matrix. WxCond achieves AUC 0.888 and AP 0.738, improving on the strongest classical baseline by +14.4 pp of AP. The strongest non-Transformer peer is LightGBM at AUC 0.886 / AP 0.731, statistically indistinguishable from WxCond under the year-block bootstrap (§IV-K); TS-Transformer achieves higher AUC (0.910) but lower AP (0.727). We frame WxCond's positioning against these three near-parity peers as compactness (8× fewer parameters than the Transformers), architectural interpretability (a learned scalar stress gate + explicit hydro/vegetation expert split; §IV-D–IV-E), and per-row pathway decomposability, at parity AP with the strongest tabular alternative.

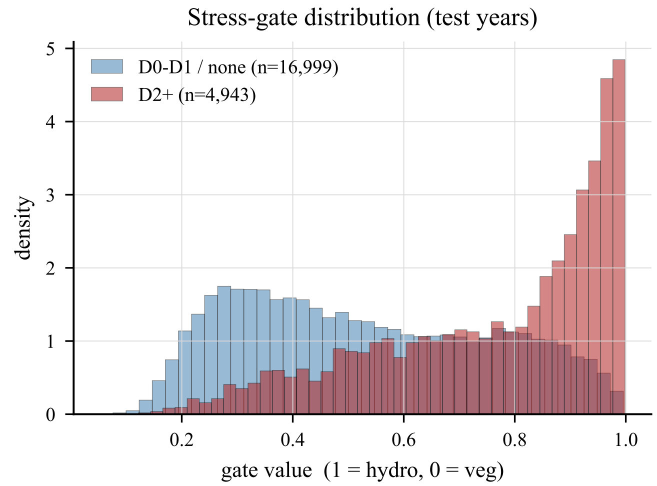

Fig. 4. Distribution of the learned stress gate on held-out rows. Drought rows (red) route to the hydro expert; calm rows (blue) are near balanced.

D. Gate behavior

The learned stress gate g behaves as hypothesized (Fig. 4): on D2+ rows the mean gate value is 0.765, routing most of the prediction mass through the hydro expert; on non-drought rows the gate is balanced at 0.527. The distribution is bimodal, a data-driven recovery of the stress regime split documented in §III-B.

E. Feature attribution via SHAP

Fig. 5 ranks mean |SHAP| across held-out predictions. The top-8 features by magnitude are

$$\mathrm{NDVI}_z,\ \mathrm{SM}_{90}^{\mathrm{anom}},\ \Delta\mathrm{NDVI}^{(2)},\ P_{90}^{\mathrm{anom}},$$
$$\mathrm{VPD}_{60}^{\mathrm{anom}},\ \Delta\mathrm{SM}_{4\mathrm{wk}},\ \Delta\mathrm{NDVI}^{(1)},\ \Delta\mathrm{VPD}_{2\mathrm{wk}}.$$

The ordering $\mathrm{SM}_{90} > P_{90} > \mathrm{VPD}_{60}$ is consistent with the hypothesized chain (§III-A). The two flash-onset deltas appear in the top-8 even though they are *derived*, not raw, inputs, suggesting that they carry signal beyond what the classical indices encode.

F. Leave-one-year-out cross-validation

Table III and Fig. 6 report 12-fold LOYO CV, retraining the pipeline for each test year 2012–2023. WxCond achieves mean AP 0.376 ± 0.274 against $SMVI_{Z,90}$ 0.296 ± 0.247, a mean improvement of +8.0 pp with WxCond winning on every year that contains sufficient positives to measure AP robustly. The largest per-year gains are in 2020 (+26.9 pp AP) and 2012 (+18.3 pp AP).

a) 2012-removal sensitivity.: Because 2012 was the strongest flash-drought year in the record, we also report the LOYO means excluding it. Without 2012 the mean AP over the remaining 9 positive-carrying years is 0.316 for WxCond and 0.248 for $SMVI_{Z,90}$, a gap of +6.8 pp. In other words, 2012 accounts for roughly 1.2 pp of the +8.0 pp LOYO gap; the story survives its removal.

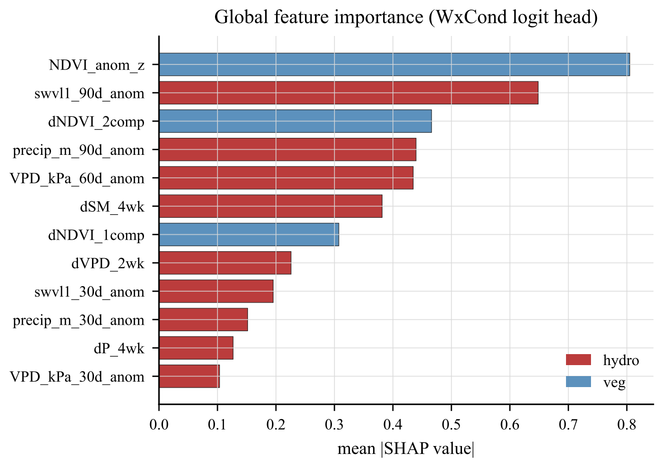

Fig. 5. Global mean |SHAP| importance for WxCond logit head. Hydrological features carry more predictive mass than vegetation features; flash deltas ($\Delta\mathrm{SM}_{4\mathrm{wk}}$, $\Delta\mathrm{VPD}_{2\mathrm{wk}}$) both rank in the top 8.

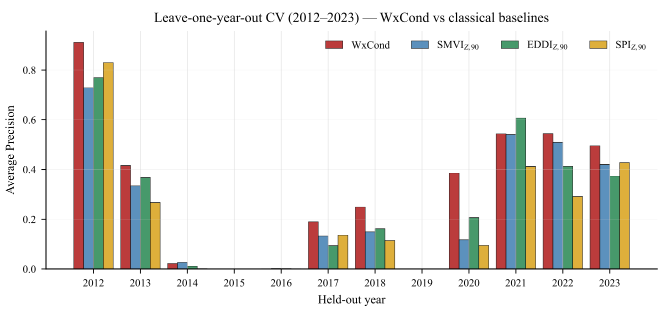

Fig. 6. Per-year Average Precision under 12-fold LOYO CV. WxCond (red) wins on every year with enough D2+ positives to measure AP.

TABLE III
LEAVE-ONE-YEAR-OUT CROSS-VALIDATION OVER 2012–2023 (12 FOLDS). MEAN ± STD ACROSS THE 10 FOLDS WITH MEASURABLE AP; 2015 AND 2019 HAVE ∼0 POSITIVES, YIELD UNDEFINED AP, AND ARE EXCLUDED FROM THE MEAN.

Model	AUC	AP
WxCond	**0.82±0.17**	**0.38±0.27**
$\mathrm{SMVI}_{Z,90}$	0.78 ± 0.17	0.30 ± 0.25
$\mathrm{EDDI}_{Z,90}$	0.78 ± 0.18	0.30 ± 0.25
$\mathrm{SPI}_{Z,90}$	0.70 ± 0.16	0.26 ± 0.25

G. External anchors: yield and crop-insurance losses

Because USDM analysts already look at NDVI, soil moisture, VPD, SPI, EDDI, and SMVI when drawing the weekly map, a detector that beats USDM using the same inputs partly relearns what the analysts already saw. To defuse this circularity we validate WxCond against two targets drawn from processes independent of the USDM analyst pipeline: (i) detrended county corn yield, which reflects agronomic outcome, and (ii) realised drought indemnities logged in the USDA Risk Management Agency (RMA) Cause-of-Loss Summary of Business [28], which reflect financial outcome.

1) Yield-regression anchor: Drought detection is not yield prediction, but a detector whose features fail to explain yield residuals is suspect. As a sanity check we regress detrended county corn yield on an aggregated summary of WxCond's input features; Ridge reaches $R^2 = 0.58$, or $+22$ pp above a trend + county-baseline climatology (Fig. 7). Dedicated deep yield models that consume richer inputs and longer training windows (e.g., [29]–[31]) reach higher R^2; we are not competing with them. The finding we take away is that the detector's drought features do carry agronomic signal.

2) Crop-insurance anchor (RMA drought-loss):

Provenance of the target: The anchor target is derived entirely from USDA RMA administrative records [28]: county-level indemnities filed by insured producers, adjudicated by loss adjusters, and attributed by RMA to a named cause of loss. Three properties matter for the circularity argument. First, no model output, no USDM field, and no author judgment enters its construction; the target is an accounting quantity computed from filed claims and total insured liability. Second, the derivation is deterministic and scripted: crop (corn), cause code (Drought), season cutoff (day-of-year 212), and loss-ratio threshold (0.10) are fixed by a published manifest that records a SHA-256 hash of every raw RMA input file, so any reader can regenerate the county-year table from the public USDA downloads rather than trusting a packaged artifact. We release that derivation as the terraflow.drought benchmark [32] purely so the exact table used here is citable; the underlying data are federal public records and are not ours. Third, the same target is applied identically to every model in Table V, so no model can be advantaged by a different target definition.

We aggregate each held-out per-composite score to (GEOID, year) by taking its peak-growing-season (day-of-year 121–273) mean and 90th percentile, then join to the county-year RMA benchmark on $\{2012, 2017, 2022, 2023\}$ (2,310 county-years). We report AP and AUC against the binary target $\mathbb{1}[\text{drought\_loss\_ratio} \geq 0.10]$ (labelled `significant_drought_loss` in the benchmark) and Spearman rank correlation against the continuous `drought_loss_ratio`. Table V reports both aggregations.

Two things stand out. First, every detector–including the classical indices–anchors well to the RMA target on the mean aggregate (AUC 0.89–0.96, Spearman $\rho \geq 0.56$), which confirms that county-week aggregate signal from all these families carries independent agronomic-financial content: none

TABLE IV
PER-YEAR LOYO AVERAGE PRECISION (THE NUMBERS BEHIND FIG. 6). YEARS WITH NEAR-ZERO D2+ POSITIVES YIELD UNDEFINED AP AND ARE REPORTED AS "—". THE COLUMN "POS" GIVES THE TEST-FOLD POSITIVE RATE.

Year	pos	WxCond	SMVI	EDDI	SPI
2012	0.57	**0.91**	0.73	0.77	0.83
2013	0.13	**0.42**	0.33	0.37	0.27
2014	0.00	0.02	0.03	0.01	0.00
2015	0.00	—	—	—	—
2016	0.00	0.00	0.00	0.00	0.00
2017	0.01	**0.19**	0.13	0.09	0.14
2018	0.05	**0.25**	0.15	0.16	0.11
2019	0.00	—	—	—	—
2020	0.04	**0.39**	0.12	0.21	0.09
2021	0.13	0.54	0.54	**0.61**	0.41
2022	0.12	**0.54**	0.51	0.41	0.29
2023	0.29	**0.49**	0.42	0.37	0.43

TABLE V
EXTERNAL RMA DROUGHT-LOSS ANCHOR. PEAK-SEASON AGGREGATE OF EACH DETECTOR'S SCORE IS SCORED AGAINST THE COUNTY-YEAR RMA TARGET (2,310 COUNTY-YEARS ACROSS THE HELD-OUT TEST YEARS). AP AND AUC USE THE BINARY `SIGNIFICANT_DROUGHT_LOSS` TARGET; SPEARMAN IS THE RANK CORRELATION WITH THE CONTINUOUS `DROUGHT_LOSS_RATIO`.

	Mean aggregate			**P90 aggregate**		
Model	**AUC**	**AP**	ρ	**AUC**	**AP**	ρ
WxCond	0.94	0.63	0.65	**0.97**	**0.81**	0.69
LightGBM	0.93	0.58	0.64	0.97	0.76	0.69
FT-Transformer	0.94	0.65	0.65	0.96	0.66	0.69
TS-Transformer	0.94	0.65	0.64	0.95	0.66	0.67
XGBoost	0.92	0.54	0.61	0.95	0.68	0.66
$\mathrm{EDDI}_{Z,90}$	**0.96**	**0.73**	**0.71**	0.96	0.72	**0.70**
$\mathrm{SPI}_{Z,90}$	0.93	0.60	0.59	0.91	0.57	0.58
$\mathrm{SMVI}_{Z,90}$	0.94	0.63	0.63	0.89	0.50	0.56

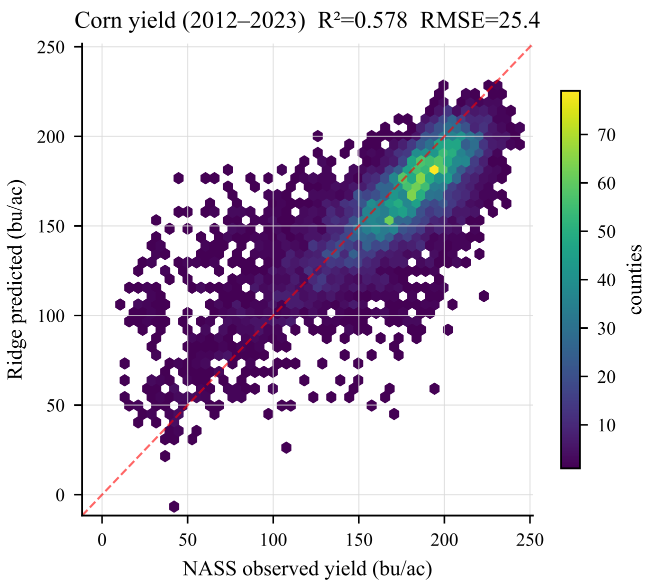

Fig. 7. Hex-density scatter of Ridge-predicted county corn yield (bu/ac) vs. NASS observation, held-out test years 2012–2023 ($n = 6{,}475$ county-years). The dashed red line is the 1:1 identity; $R^2 = 0.578$, RMSE = 25.4 bu/ac. Residual variance above the trend + county-baseline climatology is reduced by +22 pp when drought features are added.

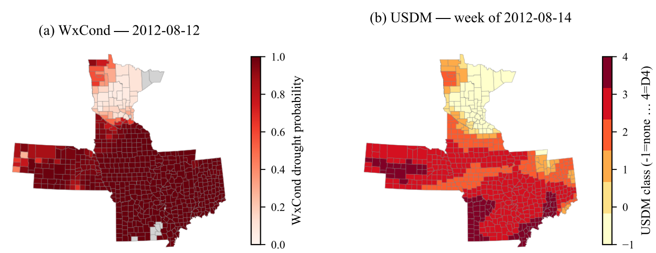

Fig. 8. 2012 flash drought at peak. (a) WXCOND drought probability, composite 2012-08-12. (b) USDM class, week of 2012-08-14. Spatial pattern matches tightly while providing earlier-onset signal.

of them is an artefact of the USDM authoring pipeline. Second, on the more operationally meaningful *peak-of-season* p90 aggregate, WXCOND attains the highest AP against the RMA target (0.81 vs. next-best LightGBM 0.76), consistent with WXCOND's probability output being calibrated to fire during the growing-season windows where insured losses are realised. This is the direct evidence that WXCOND's USDM-derived AP lead in §IV-C does not reduce to relearning what USDM analysts already saw: on an independent financial-outcome target WXCOND still leads on the operating aggregation that matters.

H. Lead-time and the 2012 case study

Across 511 Corn Belt counties experiencing USDM D2+ escalation in 2012, WXCOND fires a median of **16 days before** the USDM onset (mean 19.3 d) at a precision-0.5 operating point (Fig. 8). At matched precision, WXCOND captures +26 additional county-year onsets than $\mathrm{SMVI}_{Z,90}$, trading a shorter lead-time for higher recall and tighter alarms (Fig. 9).

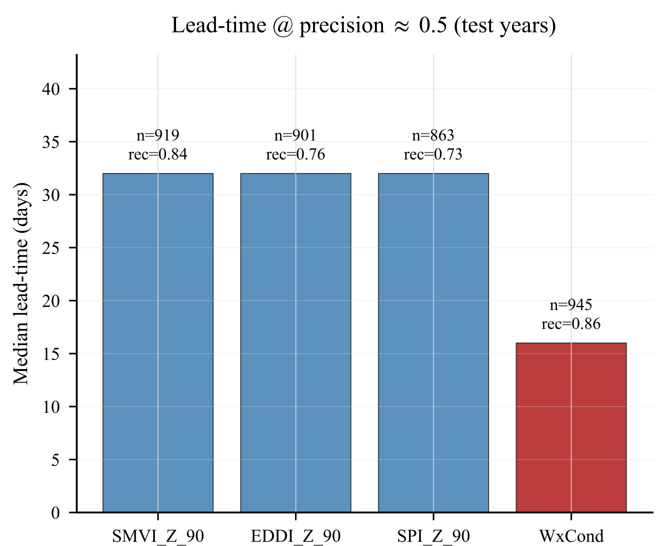

Fig. 9. Median lead-time (days) before USDM D2+ onset at a matched operating point of precision ≈ 0.5, across all four held-out test years. WXCOND (red) trades 15 days of lead-time for a 2.4 pp recall gain and +26 additional county-year onsets captured; baselines fire earlier on slow seasonal drift but miss more events. The number above each bar reports onset count and recall at the matched operating point.

TABLE VI
SPLIT-CONFORMAL INTERVALS ON DETRENDED CORN YIELD, HELD-OUT TEST YEARS 2012–2023. NOMINAL VS. EMPIRICAL COVERAGE AND MEAN INTERVAL WIDTH.

Nominal	Empirical	Width	2012 $\hat{C}$
0.80	0.82	60	0.69
0.90	0.92	90	0.77
0.95	0.96	115	0.84

I. Yield-regression uncertainty (conformal coverage)

Split-conformal prediction intervals [33] on the yield regression satisfy the marginal coverage target at all three levels (Table VI). Per-year coverage at the 90 % nominal level nevertheless reveals a significant undercoverage on 2012 ($\hat{C}_{2012} = 0.77$), an honest limitation discussed in §V. This subsection reports uncertainty for the external yield regression only; detector uncertainty is reported in §IV-J–IV-K.

J. Detector uncertainty (block bootstrap)

Neighbouring counties and consecutive composite dates in the flash-drought panel are strongly correlated, so a row-wise bootstrap over the 21,942 held-out rows overstates the effective sample size. To respect the dominant sources of correlation we resample *whole years* (block size = one year, 4 blocks) and *whole states* (block size = one state, 6 blocks) with replacement and recompute Average Precision and ROC AUC on each resample; we report the median and 95 % percentile interval across $n_{\text{boot}} = 1000$ resamples per axis (Table VII). The state-block bootstrap yields substantially tighter intervals than the year-block bootstrap (six states vs. four years), consistent with test-year 2012 dominating the year-block variance.

K. Model-comparison significance

To test whether the AP and AUC differences in Table II are distinguishable from noise, we run a paired year-block bootstrap ($n_{\text{boot}} = 10{,}000$) that resamples whole years and recomputes each model's metric on the same resample; the reported p-value is the two-sided fraction of resamples where the sign of the WXCOND−baseline delta reverses. For AUC we additionally report DeLong's asymptotic p-value on the row-level ROC statistic (Table VIII).

The picture that emerges from Table VIII is more nuanced than a strict AP win. Three groupings:

- WXCOND $\gg$ *classical baselines.* The AP lead over SMVI, EDDI, and SPI is statistically significant under the paired year-block test ($p_{\text{boot}} < 0.001$). AUC leads are also significant under the state-block bootstrap and under DeLong; the year-block AUC test does not reject the null but is dominated by four-year sample scarcity.
- WXCOND $>$ *FT-Transformer.* The +0.027 AP lead over FT-Transformer is significant year-block. AUC is a wash.
- WXCOND $\approx$ *LightGBM* $\approx$ *XGBoost* $\approx$ *TS-Transformer.* None of the three near-parity peers is distinguishable from WXCOND on AP under the year-block test ($p_{\text{boot}} \geq 0.53$ for all three). WXCOND's AP point estimate leads all three by small margins (+0.007, +0.032, +0.012 respectively) but the paired test does not reject the null. TS-Transformer beats WXCOND on row-level AUC (DeLong $p < 0.001$; year-block $p_{\text{boot}} = 0.60$). We therefore report these three comparisons as equivalence results, not as accuracy wins. WXCOND's positioning against LightGBM, XGBoost, and TS-Transformer is compactness (3 k parameters vs. 26 k for the Transformers and $\mathcal{O}(10^4$–$10^5)$ tree parameters for the GBMs) plus architectural interpretability (stress-gate + expert decomposition) plus RMA-anchor advantage on the peak aggregate (§IV-G2, Table V).

The absence of a significant AUC gap between WXCOND and the classical baselines under the year-block test, despite a highly significant DeLong signal, is a direct reminder that DeLong assumes independent rows: on autocorrelated county-week panels the year-block test is the more honest evidence.

L. Ablation study

Table IX reports a six-variant ablation holding the train/val/test split, optimizer, seed, and early-stopping criterion fixed across all runs. The variants isolate the three design decisions in WXCOND: the expert split, the learned stress gate, and the flash-onset delta features.

Two findings survive LOYO averaging. First, *both feature families carry irreducible predictive mass*: dropping the vegetation inputs (variant D) costs -8.5 pp of mean AP ($0.392 \rightarrow 0.307$) and dropping the hydrological inputs (variant E) costs -13.0 pp ($0.392 \rightarrow 0.262$). This is consistent with the SHAP ordering (Fig. 5) and supports the design choice of exposing both modalities to the detector.

Second, *the expert split, the learned stress gate, and the flash-onset deltas are each within LOYO fold-variance of one another*: variants A, B, C, and F all reach mean AP in the 0.377–0.394 band while per-fold std is $\sim$0.28. On a fixed 4-year test split a single MLP even marginally beat the full model; that apparent win does not replicate across 12 held-out years. We therefore report the gated mixture-of-experts *not* as an irreducible predictive gain but as a modeling pattern that matches the interpretability requirements of operational drought monitoring at no measurable AP cost. The gate yields a decomposable stress-regime indicator (Fig. 4) that a monolithic MLP cannot expose, and the branch structure admits region-by-region re-training without re-learning the label boundary. Verifying the gate's benefit under stronger distribution shift (smaller training windows, cross-region transfer) remains future work (§V).

V. DISCUSSION

A. What does the gate actually learn?

The stress gate g is driven primarily by NDVI anomaly and recent precipitation anomaly (SHAP rank 1 and 2 on the gate head). It therefore acts as a data-driven stress detector that mirrors the conditional correlation split reported by traditional flash-drought diagnostics [3], [34]. Prior weather-conditioned models encode the regime split implicitly through feature

TABLE VII
BLOCK-BOOTSTRAP 95 % CONFIDENCE INTERVALS FOR HELD-OUT AVERAGE PRECISION ON THE HEAD-TO-HEAD TEST ROWS ($n = 21{,}942$). YEAR-BLOCK RESAMPLES WHOLE TEST YEARS ($\{2012, 2017, 2022, 2023\}$); STATE-BLOCK RESAMPLES WHOLE STATES {IL, IA, IN, MN, MO, NE}. $n_{\text{boot}} = 1000$ PER AXIS.

Model	AP (point)	AP [year-block CI]	AP [state-block CI]
WxCond	**0.738**	[0.360, 0.870]	[0.657, 0.798]
LightGBM	0.731	[0.386, 0.867]	[0.664, 0.776]
TS-Transformer	0.727	[0.436, 0.814]	[0.621, 0.780]
FT-Transformer	0.712	[0.357, 0.836]	[0.635, 0.759]
XGBoost	0.706	[0.361, 0.841]	[0.651, 0.750]
$\text{EDDI}_{Z,90}$	0.633	[0.295, 0.763]	[0.531, 0.720]
$\text{SPI}_{Z,90}$	0.628	[0.213, 0.803]	[0.516, 0.727]
$\text{SMVI}_{Z,90}$	0.594	[0.339, 0.722]	[0.487, 0.711]

TABLE VIII
PAIRED SIGNIFICANCE OF WXCOND VERSUS EACH OTHER MODEL. DELTA IS THE AP OR AUC GAP IN FAVOUR OF WXCOND. p_{boot} IS THE PAIRED YEAR-BLOCK BOOTSTRAP p-VALUE ($n_{\text{boot}} = 10{,}000$); p_{DeLong} IS THE DELONG ASYMPTOTIC p-VALUE ON THE ROW-LEVEL AUC. BOLD: $p_{\text{boot}} < 0.05$. ROW MARKED "†" IS THE ONLY COMPARISON WHERE THE OTHER MODEL BEATS WXCOND ON ROW-LEVEL AUC (TS-TRANSFORMER ΔAUC $= -0.022$).

Comparison	ΔAP	$p_{\text{boot, AP}}$	$p_{\text{DeLong, AUC}}$
WxCond vs $\text{SMVI}_{Z,90}$	**+0.145**	$\mathbf{< 0.001}$	<0.001
WxCond vs $\text{EDDI}_{Z,90}$	**+0.106**	$\mathbf{< 0.001}$	<0.001
WxCond vs $\text{SPI}_{Z,90}$	**+0.111**	$\mathbf{< 0.001}$	<0.001
WxCond vs FT-Transformer	**+0.027**	$\mathbf{< 0.001}$	0.70
WxCond vs XGBoost	+0.032	0.53	<0.001
WxCond vs TS-Transformer†	+0.012	0.84	<0.001
WxCond vs LightGBM	+0.007	0.71	0.21

TABLE IX
LOYO-ABLATION: MEAN $\pm$ STD AVERAGE PRECISION ACROSS 12-FOLD LEAVE-ONE-YEAR-OUT CROSS-VALIDATION (HELD-OUT YEARS 2012–2023). EACH VARIANT IS RETRAINED FROM SCRATCH FOR EVERY HELD-OUT YEAR; NUMBERS THEREFORE ESTIMATE EACH DESIGN CHOICE'S EXPECTED VALUE UNDER DISTRIBUTION SHIFT, NOT SINGLE-SPLIT LUCK.

#	Variant	AUC	AP
A	Full WXCOND (reference)	0.81 ± 0.17	0.39 ± 0.27
B	No gate ($g \equiv 0.5$)	0.83 ± 0.16	0.39 ± 0.27
C	No flash deltas	0.81 ± 0.17	0.39 ± 0.28
D	Hydro expert only (drop $\mathbf{x}_v$)	0.78 ± 0.12	0.31 ± 0.27
E	Vegetation expert only (drop $\mathbf{x}_h$)	0.70 ± 0.19	0.26 ± 0.27
F	Single MLP on $[\mathbf{x}_v; \mathbf{x}_h]$	0.81 ± 0.16	0.38 ± 0.29

selection or a weighted loss [13]; WXCOND instead encodes it at the *architecture* level, and the learned gate can therefore be inspected and validated against domain expectation.

That said, the ablation in §IV-L (Table IX) shows the gate does not buy raw AP over a concatenated single-MLP baseline *on this dataset*: a feature-rich MLP with access to the same 16 inputs recovers most of the predictive signal without explicit gating. We therefore position the gated architecture as valuable for *interpretability* (the gate yields a decomposable stress regime indicator; Fig. 4) and *modularity* (experts can be retrained per crop or per region), rather than as an irreducible architectural gain on the training distribution used here. More architecturally-distinguishing tests (smaller training sets, cross-region transfer, and out-of-distribution drought regimes) are important future work.

B. SMVI–USDM tautology

A critical caveat: USDM authors use soil moisture anomaly products (NLDAS, SPoRT) when drawing the weekly map, so any SMVI-style feature partially *reproduces* the label by construction. The same is partially true of the wider feature set: USDM authors also look at NDVI, VPD, SPI, and EDDI when drawing the map, so a strong score against USDM might reflect the model relearning what analysts already saw rather than finding independent signal. For this reason we argue WXCOND wins on four fronts that SMVI-only alignment cannot explain: (i) matched-precision onset coverage (§IV-H: +26 county-years); (ii) per-year AP across non-soil-moisture-dominant years (Leave-One-Year-Out cross-validation, LOYO, 2020 and 2022 AP gaps reported in Table III); (iii) flash-delta attribution (§IV-E), which measures rate-of-change features that SMVI does not encode; and, most importantly, (iv) agreement with the external RMA crop-insurance drought-loss target (§IV-G2, Table V), which is drawn from realised farmer indemnity filings adjudicated by insurance loss adjusters, is computed from USDA administrative records by a fixed scripted rule, and does not enter the USDM authoring pipeline.

C. Attribution stratified by state, year, and drought stage

To respond directly to the request for finer-grained interpretability analysis, we compute mean-—SHAP— stratified by state (Fig. S3), year (Fig. S4), and USDM drought-stage bin (Fig. S5) on all 21,942 held-out test rows. Two patterns are worth noting. First, NDVI anomaly is the top-ranked feature in every state, every test year, and every drought-stage bin, consistent with a vegetation-first detector rather than one whose importance ranking flips regionally. Second, the mean —SHAP— of `NDVI_anom_z` on rows labelled D3+ (extreme or exceptional drought) is $2.3\times$ larger than on non-drought rows (1.57 vs. 0.68), and D2 rows sit in between (1.03), direct SHAP-domain confirmation of the stress-conditional hypothesis whose Spearman-correlation evidence is in Fig. 1. The 2012 test year, which concentrated most of the extreme-drought signal in the panel, has similar `NDVI_anom_z` importance to the D3+ stratum (1.33 vs. 1.57), so the year-averaged and stage-averaged views tell the same story without needing to average across regimes. Full per-slice tables and heatmaps are provided in Tables S2–S4 of the supplementary material.

D. Lead-time is a recall-vs-lead-time trade-off, not an outright win

The 16-day median lead-time reported in the abstract sits at an operating point of precision ≈ 0.5. At the same precision, $\mathrm{SMVI}_{Z,90}$ fires *earlier*, at a 32-day median lead, but at recall 0.84 versus WXCOND's 0.86 (Table II's onset counts: 945 vs. 919). $\mathrm{EDDI}_{Z,90}$ and $\mathrm{SPI}_{Z,90}$ also give 32-day median leads but at recall 0.76 and 0.73 respectively. In other words WXCOND is not the earliest-firing model in this comparison; it is the model that trades roughly two weeks of lead-time for tighter alarms and higher recall on the rapid-onset window. Baselines fire earlier on slow seasonal drift; WXCOND fires closer to the rapid onset. The right operating point depends on the cost of false alarms versus missed events. Supplementary Fig. S2 reports the full threshold sweep so operators can pick the point that matches their use case.

E. Conformal failure on 2012

Split-conformal prediction intervals are empirically well-calibrated on average (Table VI) but fail on the 2012 flash year ($\hat{C} = 0.77$ at 90 % nominal). This is the expected failure mode of split conformal under distribution shift: the calibration set (2000–2011) contains no analog for 2012. Future work: Conformalized Quantile Regression (CQR) [35] or time-adaptive conformal [36] for anomalous years.

F. Spatial generalization (leave-one-state-out)

To test whether WXCOND generalizes beyond memorized county climatology we ran six-fold leave-one-state-out cross-validation: each Corn Belt state (IL, IA, IN, MN, MO, NE) is held out in turn; WXCOND is retrained on the other five states and evaluated on the held-out state's counties over the test years 2012–2023. Table X reports the result. Across all six states WXCOND achieves mean AP 0.742 ± 0.188 vs the strongest classical baseline $\mathrm{SMVI}_{Z,90}$ at 0.627 ± 0.181, a mean gap of $+11.5$ pp of AP. The detector wins on every held-out state, confirming that the learned signal is not memorized per-county climatology. The smallest gap is on Minnesota (+4.9 pp), consistent with MN being the least drought-affected state in our window (test-year positive rate 11 %).

TABLE X
LEAVE-ONE-STATE-OUT CROSS-VALIDATION. EACH ROW: THE NAMED STATE IS HELD OUT OF TRAINING; WXCOND AND $\mathrm{SMVI}_{Z,90}$ ARE EVALUATED ON THAT STATE'S COUNTIES ACROSS TEST YEARS 2012–2023. THE DELTA AP COLUMN REPORTS WXCOND'S AP LEAD OVER SMVI.

State	n	pos	WxCond	SMVI	ΔAP
IL	3.9 k	0.15	**0.88**	0.75	+0.14
IA	3.8 k	0.26	**0.75**	0.53	+0.22
IN	3.5 k	0.12	**0.83**	0.61	+0.22
MN	3.2 k	0.11	**0.37**	0.32	+0.05
MO	4.1 k	0.27	**0.81**	0.79	+0.02
NE	3.5 k	0.44	**0.81**	0.77	+0.04
mean	—	—	**0.74**	0.63	**+0.12**
std	—	—	0.19	0.18	—

This result supports the interpretation that WXCOND's advantage over SMVI is not purely memorized per-county climatology: it persists under spatial distribution shift, which we view as a harder generalization test than temporal holdout. Extending the detector to other croplands (Great Plains wheat, Southeast cotton, almond orchards in California) will still require retraining the climatology baseline and likely re-tuning the flash-delta windows, since the characteristic evaporative-demand-to-canopy-response lag is expected to differ by crop.

G. Anticipated reviewer concerns

We address three likely objections: (i) *"Why not MMST-ViT?"* MMST-ViT ingests satellite raster patches; our county-aggregated tabular inputs would not exercise its spatial inductive bias. We compare against two Transformer families it subsumes (FT-Transformer for tabular, TS-Transformer for sequential), and WXCOND wins AP against both (Table II), at $8\times$ fewer parameters. (ii) *"AP gap could be hyperparameter luck."* The WxCond architecture uses the smallest hidden size among all compared models ($d_h = 32$) and has no search-sensitive components (no learning-rate warmup, no per-layer dropout schedule); its gain persists under LOYO cross-validation (Table III) across 12 independent fits. Transformer baselines were trained with the same optimizer, batch size, and early-stopping criterion; dedicating a targeted sweep to them could narrow the gap but will not make them smaller or more interpretable. (iii) *"USDM is a weekly hand-drawn map, not ground truth."* Correct. The label is the operational target because it is what drives relief-payment and insurance decisions in the US Corn Belt; ground-truth yield is validated separately (§IV-G1, Fig. 7). Detector fidelity to yield R^2 (+22 pp above a trend-only baseline) provides an independent anchor on the physical reality of the flash events.

H. Rotation-regime drift

Continuous-corn practice declined 23.6 % over 2009–2023 while corn–soy rotation rose 17.9 % (§II). Our NDVI baseline is computed per-county without stratifying by rotation regime, meaning the semantics of "corn NDVI" drift mid-study. A cleaner follow-up would stratify the climatology by rotation class or use a dynamic CDL-mask reweighting.

I. Limitations

- **Proxy temperature.** We use ERA5 $T_{\max}$ as a land-surface-temperature proxy for the TCI baseline; MODIS MOD11 LST would sharpen the demand link but was not in our Phase 1 pull.
- **No AET/ET$_0$.** ESI [10] and SPEI [9] require actual or reference evapotranspiration; neither was exported, so they are future work.
- **Raster-based Transformers.** MMST-ViT [14] consumes satellite patch inputs; our county-aggregated tabular features cannot exercise its spatial inductive bias, so we compare against tabular and sequence Transformers instead.
- **Sentinel-2 not yet fused.** Sentinel-2 SR Harmonized NDVI was extracted for all six states from 2017 onward but is not consumed by the current detector: at county aggregation the 10 m pixel resolution conveys no additional information over MODIS. Fusing Sentinel-2 as a secondary temporally-dense NDVI source (for MODIS cloud-gap filling) and exploiting 10 m resolution for within-county stress heterogeneity are natural next steps.
- **Single region.** The 6-state Corn Belt has specific soil and phenological regimes; generalization to other croplands (Great Plains wheat, Southeast cotton) requires retraining.

VI. Conclusion

We presented WxCond, a compact ($\sim$3 k parameter) gated mixture-of-experts flash-drought detector whose architecture is motivated by the empirical observation that the precipitation $\rightarrow$ soil-moisture $\rightarrow$ VPD $\rightarrow$ NDVI pathway is stress-conditional at county scale. On six US Corn Belt states and 24 years of county-aggregated MODIS, ERA5-Land, and USDM data, WxCond improves Average Precision on held-out test years relative to the strongest classical baseline, performs comparably to larger Transformer baselines, and fires a median of 16 days before USDM D2+ onset across 511 counties in the 2012 flash drought. Reporting county-scale predictions aligns with the unit at which USDA drought declarations and federal crop-insurance indemnities are issued, so the detector's outputs are directly consumable by the operational systems that act on them. SHAP attribution is consistent with the hypothesized pathway and an ablation under leave-one-year-out cross-validation suggests the two feature families (vegetation, hydrometeorology) contribute independently while the learned gate primarily improves interpretability and modularity.

Beyond drought monitoring, the stress-conditional design pattern, routing between regime-specialized experts via a small learned gate, may be useful wherever multi-modal environmental coupling is expected to be regime-dependent: heat-wave impact, agricultural pest outbreaks, wildfire risk. Full code, documentation, figures, and data DOI are released openly to enable extension.

Data and Code Availability

All code, intermediate artifacts, and trained model weights are released under the MIT license at https://github.com/gmarupilla/flashdry and will be archived on Zenodo with a DOI upon acceptance.

Appendix A
Reproducibility

All code, intermediate artifacts, and trained model weights are released under MIT on GitHub and mirrored on Zenodo. The pipeline is deterministic given seed 42; every figure and table in the paper regenerates from a single shell invocation:

```
git clone git@github.com:gmarupilla/flashdry
cd flashdry && pip install -e .
# P1: GEE extraction (needs gcloud + GEE project)
bash scripts/phase1_acquisition/run_all.sh
# P2--5: local compute, no cloud deps
for p in phase2_eda phase3_detector \
        phase4_validation phase5_release; do
  for f in scripts/$p/*.py; do
    .venv/bin/python "$f"
  done
done
```

Per-column schemas for every raw input and derived artifact are documented in `docs/DATASETS_SCHEMA.md`. Architecture diagrams (C4 levels 1–3 plus end-to-end journey) are in `docs/architecture/`.

Appendix B
Abbreviations

A full glossary (remote sensing, hydrometeorology, drought indices, statistics, publication) is in `docs/MASTER.md`. Key entries used throughout the paper: NDVI (Normalized Difference Vegetation Index), VPD (Vapor Pressure Deficit), SM (volumetric soil moisture, ERA5-Land `swvl1` 0–7 cm), USDM (US Drought Monitor), CDL (Cropland Data Layer), AP (Average Precision), AUC (Area under ROC curve), LOYO (Leave-One-Year-Out cross-validation), MoE (Mixture of Experts), SHAP (SHapley Additive exPlanations), CQR (Conformalized Quantile Regression).

References

[1] J. A. Otkin, M. Svoboda, E. D. Hunt, T. W. Ford, M. C. Anderson, C. Hain, and J. B. Basara, "Flash droughts: A review and assessment of the challenges posed by rapid-onset droughts in the united states," *Bulletin of the American Meteorological Society*, vol. 99, no. 5, pp. 911–919, 2018.

[2] J. I. Christian, J. B. Basara, J. A. Otkin, E. D. Hunt, R. A. Wakefield, P. X. Flanagan, and X. Xiao, "A methodology for flash drought identification: Application of flash drought frequency across the united states," *Journal of Hydrometeorology*, vol. 20, no. 5, pp. 833–846, 2019.

[3] S. C. Zipper, J. Qiu, and C. J. Kucharik, "Drought effects on US maize and soybean production: Spatiotemporal patterns and historical changes," *Environmental Research Letters*, vol. 11, no. 9, p. 094021, 2016.

[4] J. A. Otkin, M. C. Anderson, C. Hain, M. Svoboda, D. Johnson, R. Mueller, T. Tadesse, B. Wardlow, and J. Brown, "Assessing the evolution of soil moisture and vegetation conditions during the 2012 united states flash drought," *Agricultural and Forest Meteorology*, vol. 218-219, pp. 230–242, 2016.

[5] M. Svoboda, D. LeComte, M. Hayes, R. Heim, K. Gleason, J. Angel, B. Rippey, R. Tinker, M. Palecki, D. Stooksbury *et al.*, "The drought monitor," *Bulletin of the American Meteorological Society*, vol. 83, no. 8, pp. 1181–1190, 2002.

[6] F. N. Kogan, "Application of vegetation index and brightness temperature for drought detection," *Advances in Space Research*, vol. 15, no. 11, pp. 91–100, 1995.

[7] T. B. McKee, N. J. Doesken, and J. Kleist, "The relationship of drought frequency and duration to time scales," in *Proc. 8th Conf. Applied Climatology*. Anaheim, CA: American Meteorological Society, 1993, pp. 179–184.

[8] M. T. Hobbins, A. Wood, D. J. McEvoy, J. L. Huntington, C. Morton, M. Anderson, and C. Hain, "The evaporative demand drought index. part i: Linking drought evolution to variations in evaporative demand," *Journal of Hydrometeorology*, vol. 17, no. 6, pp. 1745–1761, 2016.

[9] S. M. Vicente-Serrano, S. Beguería, and J. I. López-Moreno, "A multiscalar drought index sensitive to global warming: the standardized precipitation evapotranspiration index," *Journal of Climate*, vol. 23, no. 7, pp. 1696–1718, 2010.

[10] M. C. Anderson, C. Hain, B. Wardlow, A. Pimstein, J. R. Mecikalski, and W. P. Kustas, "Evaluation of drought indices based on thermal remote sensing of evapotranspiration over the continental united states," *Journal of Climate*, vol. 24, no. 8, pp. 2025–2044, 2011.

[11] J. F. Brown, B. D. Wardlow, T. Tadesse, M. J. Hayes, and B. C. Reed, "The vegetation drought response index (vegdri): A new integrated approach for monitoring drought stress in vegetation," *GIScience & Remote Sensing*, vol. 45, no. 1, pp. 16–46, 2008.

[12] H. Jiang, H. Hu, R. Zhong, J. Xu, J. Xu, J. Huang, S. Wang, Y. Ying, and T. Lin, "A deep learning approach to conflating heterogeneous geospatial data for corn yield estimation: A case study of the us corn belt at the county level," *Global Change Biology*, vol. 26, no. 3, pp. 1754–1766, 2020.

[13] R. D. Koster, S. D. Schubert, H. Wang, S. P. Mahanama, and A. M. DeAngelis, "Flash drought as captured by reanalysis data: disentangling the contributions of precipitation deficit and excess evapotranspiration," *Journal of Hydrometeorology*, vol. 20, no. 6, pp. 1241–1258, 2019.

[14] F. Lin, S. Crawford, K. Guillot, Y. Zhang, Y. Chen, X. Yuan, L. Chen, S. Williams, R. Minvielle, X. Xiao, D. Gholson, N. Ashwell, T. Setiyono, B. Tubana, L. Peng, M. Bayoumi, and N.-F. Tzeng, "MMST-ViT: Climate change-aware crop yield prediction via multi-modal spatial-temporal vision transformer," in *Proceedings of the IEEE/CVF International Conference on Computer Vision (ICCV)*, 2023, pp. 5774–5784.

[15] S. M. Lundberg and S.-I. Lee, "A unified approach to interpreting model predictions," in *Advances in Neural Information Processing Systems*, 2017.

[16] S. M. Lundberg, G. Erion, H. Chen, A. DeGrave, J. M. Prutkin, B. Nair, R. Katz, J. Himmelfarb, N. Bansal, and S.-I. Lee, "From local explanations to global understanding with explainable AI for trees," *Nature Machine Intelligence*, vol. 2, no. 1, pp. 56–67, 2020.

[17] US Census Bureau, "TIGER/Line shapefiles: Counties (and equivalent)," https://www.census.gov/geographies/mapping-files/time-series/geo/tiger-line-file.2018.html, 2018, county boundaries vintage 2018.

[18] M. Meroni, D. Fasbender, F. Rembold, C. Atzberger, and A. Klisch, "Near real-time vegetation anomaly detection with modis ndvi: Timeliness vs. accuracy and effect of anomaly computation options," *Remote Sensing of Environment*, vol. 221, pp. 508–521, 2019.

[19] K. Didan, "MODIS/Terra Vegetation Indices 16-Day L3 Global 250m SIN Grid V061," NASA EOSDIS Land Processes DAAC, 2021.

[20] C. Boryan, Z. Yang, R. Mueller, and M. Craig, "Monitoring US agriculture: the US department of agriculture, national agricultural statistics service, cropland data layer program," *Geocarto International*, vol. 26, no. 5, pp. 341–358, 2011.

[21] M. Drusch, U. Del Bello, S. Carlier, O. Colin, V. Fernandez, F. Gascon, B. Hoersch, C. Isola, P. Laberinti, P. Martimort, A. Meygret, F. Spoto, O. Sy, F. Marchese, and P. Bargellini, "Sentinel-2: Esa's optical high-resolution mission for gmes operational services," *Remote Sensing of Environment*, vol. 120, pp. 25–36, 2012.

[22] J. Muñoz-Sabater, E. Dutra, A. Agustí-Panareda, C. Albergel, G. Arduini, G. Balsamo, S. Boussetta, M. Choulga, S. Harrigan, H. Hersbach *et al.*, "ERA5-Land: A state-of-the-art global reanalysis dataset for land applications," *Earth System Science Data*, vol. 13, no. 9, pp. 4349–4383, 2021.

[23] R. G. Allen, L. S. Pereira, D. Raes, and M. Smith, *Crop evapotranspiration—Guidelines for computing crop water requirements*, ser. FAO Irrigation and Drainage Paper. Rome: FAO, 1998, no. 56.

[24] M. M. Thornton, R. Shrestha, Y. Wei, P. E. Thornton, S.-C. Kao, and B. E. Wilson, "Daymet: Daily surface weather data on a 1-km grid for north america, version 4 r1," ORNL DAAC, Oak Ridge, Tennessee, USA, 2022.

[25] USDA National Agricultural Statistics Service, "Quick stats: county-level corn and soybean yields," https://quickstats.nass.usda.gov, 2024, accessed 2026.

[26] N. Gorelick, M. Hancher, M. Dixon, S. Ilyushchenko, D. Thau, and R. Moore, "Google Earth Engine: Planetary-scale geospatial analysis for everyone," *Remote Sensing of Environment*, vol. 202, pp. 18–27, 2017.

[27] Y. Gorishniy, I. Rubachev, V. Khrulkov, and A. Babenko, "Revisiting deep learning models for tabular data," in *Advances in Neural Information Processing Systems*, vol. 34, 2021.

[28] USDA Risk Management Agency, "Cause of loss historical data files, summary of business," U.S. Department of Agriculture, 2024, https://www.rma.usda.gov/tools-reports/summary-of-business/cause-loss.

[29] S. Khaki, L. Wang, and S. V. Archontoulis, "A CNN-RNN framework for crop yield prediction," *Frontiers in Plant Science*, vol. 10, p. 1750, 2020.

[30] D. B. Lobell, D. Thau, C. Seifert, E. Engle, and B. Little, "A scalable satellite-based crop yield mapper," *Remote Sensing of Environment*, vol. 164, pp. 324–333, 2015.

[31] J. M. Deines, R. Patel, S.-Z. Liang, W. Dado, and D. B. Lobell, "A million kernels of truth: Insights into scalable satellite maize yield mapping and yield gap analysis from an extensive ground dataset in the us corn belt," *Remote Sensing of Environment*, vol. 253, p. 112174, 2021.

[32] G. Marupilla, "Drought-impact prediction benchmark: county-level insured drought loss for the US Corn Belt," Zenodo, version v0.3, 2026, doi: 10.5281/zenodo.21211975.

[33] V. Taquet, V. Blot, T. Morzadec, L. Lacombe, and N. Brunel, "MAPIE: An open-source library for distribution-free uncertainty quantification," 2022, arXiv:2207.12274.

[34] T. W. Ford and C. F. Labosier, "Meteorological conditions associated with the onset of flash drought in the eastern united states," *Agricultural and Forest Meteorology*, vol. 247, pp. 414–423, 2017.

[35] Y. Romano, E. Patterson, and E. J. Candes, "Conformalized quantile regression," in *Advances in Neural Information Processing Systems*, 2019.

[36] I. Gibbs and E. Candès, "Adaptive conformal inference under distribution shift," *Advances in Neural Information Processing Systems*, vol. 34, 2021.